CHINESE OPTICS LETTERS

Vol. 22, No. 3 | March 2024

Enhancing the ability of single-pixel imaging against the source's energy fluctuation by complementary detection

Junjie Cai (蔡俊杰)[1,2] and Wenlin Gong (龚文林)[1,2*]

[1] School of Optoelectronic Science and Engineering, Soochow University, Suzhou 215006, China

[2] Key Laboratory of Modern Optical Technologies of the Ministry of Education, Soochow University, Suzhou 215006, China

*Corresponding author: wlgong@suda.edu.cn

Received October 19, 2023 | Accepted October 27, 2023 | Posted Online March 22, 2024

The source's energy fluctuation has a great effect on the quality of single-pixel imaging (SPI). When the method of complementary detection is introduced into an SPI camera system and the echo signal is corrected with the summation of the light intensities recorded by two complementary detectors, we demonstrate, by both experiments and simulations, that complementary single-pixel imaging (CSPI) is robust to the source's energy fluctuation. The superiority of the CSPI structure is also discussed in comparison with previous SPI via signal monitoring.

Keywords: computational imaging; image reconstruction; complementary detection; correlation function.
DOI: 10.3788/COL202422.031101

1. Introduction

In comparison with point-to-point scanning imaging with a single-pixel detector, single-pixel imaging (SPI) can staringly obtain the image of an unknown object by computing the correlation function between the intensity of the modulation field and the target's transmitted/reflected intensity recorded by a detector without spatial resolution[1–8]. At present, there are two typical schematics for SPI[7,8]. One is computational ghost imaging (CGI), where the target is illuminated by a series of speckle patterns, and the photons reflected from the target are collected onto a single-pixel detector[9–11]. The other is single-pixel camera (SPC), where the target is usually imaged onto a spatial modulation device and the modulated signals are received by a single-pixel detector[5,6]. Recently, some works have demonstrated that SPC has some obvious advantages in comparison with CGI and have attracted much more attention[7,8,12–14]. For example, the structure of SPC usually satisfies the process of bucket detection in long-range imaging, and the reconstruction algorithm via compressive sensing is always valid[8,12]. For another example, the detection range of CGI Lidar is limited by the damage threshold of the modulation device, whereas there is no need for the SPC to be considered because the reflection signal is usually weak[13]. In addition, the SPC is superior to CGI in the same light disturbance environment, and the structure's size of the SPC is usually smaller than that of CGI[14].

Different from conventional imaging, both the property of the coded speckle patterns and the detection signal-to-noise ratio have a great influence on the quality of SPI[15–20]. In order to guarantee a good imaging quality in the case of a relatively low sampling rate (namely, the measurement number used for image reconstruction is smaller than the pixel number of the image), some common orthogonal encodings, like the Hadamard matrix and orthogonal Gaussian matrix, are usually adopted for the modulation of the light field[15–19]. However, orthogonal-code patterns are much more sensitive to noise compared with other random code patterns and the source's energy is required to be stable enough during the whole sampling process[20,21]. If the source's energy is unstable, then the energy fluctuation is equivalent to a random multiplicative noise, which will lead to rapid degradation of SPI quality[21]. In order to overcome the issue above, a monitor is usually introduced to measure the source's energy fluctuation and corresponding correction approaches have been raised[14,21]. In contrast with the method in Ref. [21], the scheme of Fig. 1(b) described in Ref. [14] is much better because the energy fluctuation of both the source and the light disturbance is measured. However, the signal recorded by the monitor should be strong enough so that the energy fluctuation can be precisely measured, which is difficult in the applications of remote sensing and weak light imaging. Therefore, it is natural to ask whether there are other superior SPI schemes against the energy fluctuation. In this paper, based on the principle of complementary detection[22–24], we have investigated the effect of the source's energy fluctuation on the quality of complementary single-pixel imaging (CSPI), and the corresponding signal correction method has been proposed to further enhance the quality of CSPI. What is more, the validity of CSPI against the source's energy fluctuation is verified by

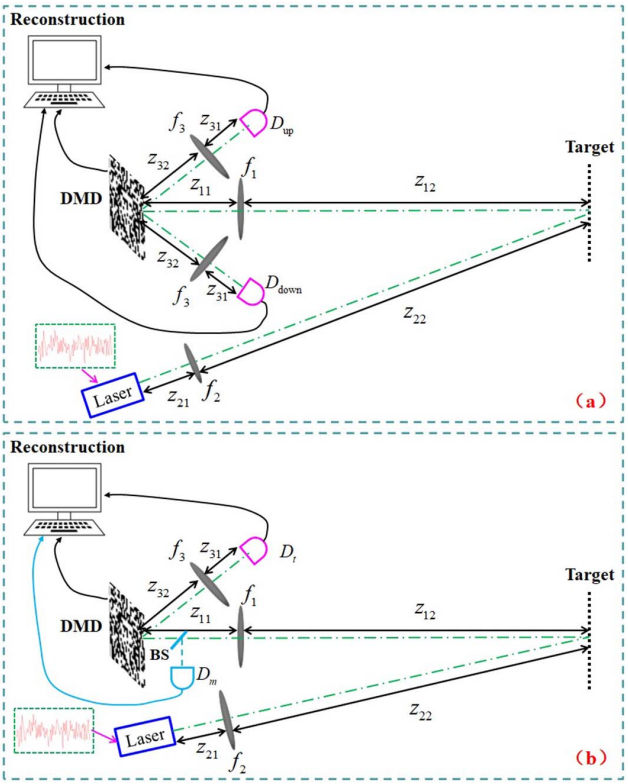

Fig. 1. (a) Proof-of-principle schematic of complementary single-pixel imaging against the source's energy fluctuation and (b) a previous method used for discussion.

experiments, and its advantages are also discussed in comparison with previous SPI via signal monitoring.

2. Model and Image Reconstruction

The digital micro-mirror device (DMD), as a high-speed light modulator, is widely used for the SPI system[6–8]. By controlling the micro-mirrors of the DMD, we can obtain a series of random binary code patterns with different statistical distributions[16–20]. However, the energy utilization rate of these amplitude modulation methods is 50%. Based on the modulation property of the DMD, the approach of complementary detection is adopted to enhance the quality of SPI[22–24]. Figure 1(a) presents the standard schematic of CSPI. The light emitted from a laser uniformly illuminates the target and the target is imaged onto a DMD by an optical imaging system with the focal length f_1. By controlling the mirrors of the DMD, the target's image is modulated and then the photons reflected by the DMD are collected onto two single-pixel detectors, D_{up} and D_{down}, by using another two conventional imaging systems with the focal length f_3, respectively. According to the property of the DMD, the patterns at the plane of the detectors D_{up} and D_{down} are complementary. In this paper, we consider that the intensity of the laser on the target plane is spatially uniform, but its intensity is different for each measurement. The intensity Y^i_{up} recorded by the detector D_{up} can be represented as[25]

$$Y^i_{up} = I^i \int A^i(x)T(x)\mathrm{d}x + I^i_{n-up}, \quad \forall_i = 1, \ldots, K, \tag{1}$$

where I^i and $A^i(x)$ denote the intensity of the laser on the target plane and the distribution of the pattern modulated by the DMD for the ith measurement, respectively. In addition, $T(x)$ is the intensity reflection function of the target, and K is the total measurement number. I^i_{n-up} is the detection noise of the detector D_{up} for the ith measurement.

Because the detection process of Fig. 1(a) is complementary, the intensity Y^i_{down} recorded by the detector D_{down} can be described as

$$Y^i_{down} = I^i \int (1 - A^i(x))T(x)\mathrm{d}x + I^i_{n-down}, \quad \forall_i = 1, \ldots, K, \tag{2}$$

where I^i_{n-down} is the detection noise of the detector D_{down} for the ith measurement.

According to the principle of SPI, the target's image O_{SPI} can be reconstructed by computing the correlation function between the pattern's intensity distributions $A^i_s(x)$ modulated by the DMD and the detector recorded intensities Y^i_s[8,14],

$$O^s_{SPI}(x) = \frac{1}{K}\sum_{i=1}^{K}(A^i_s(x) - \langle A_s(x)\rangle)Y^i_s, \quad s = \mathrm{up}, \mathrm{down}, \tag{3}$$

where $\langle A_s(x)\rangle = \frac{1}{K}\sum_{s=1}^{K} A^i_s(x)$ represents the ensemble average of $A^i_s(x)$, $A^i_{up}(x) = A^i(x)$, and $A^i_{down}(x) = 1 - A^i(x)$. Previous works have demonstrated that the quality of both $O^{up}_{SPI}(x)$ and $O^{down}_{SPI}(x)$ will be rapidly degraded when the intensity fluctuation [namely, $\delta = \frac{\mathrm{std}(I^i)}{\langle I^i\rangle}$, where $\mathrm{std}(I^i)$ denotes the standard deviation of the vector I^i] of the light field illuminating on the target is increased, especially when $\delta > 0.05$[14,21]. Based on the idea of complementary detection[22], the image of CSPI [namely, $O_{CSPI}(x)$] is the summation of the reconstruction results of $O^{up}_{SPI}(x)$ and $O^{down}_{SPI}(x)$. By some deviations, $O_{CSPI}(x)$ can be achieved by computing the correlation function between the pattern's intensity distributions $A^i(x)$ and Y^i_{CSPI}, namely,

$$O_{CSPI}(x) = O^{up}_{SPI}(x) + O^{down}_{SPI}(x) = \frac{1}{K}\sum_{i=1}^{K}(A^i(x) - \langle A(x)\rangle)Y^i_{CSPI}, \tag{4}$$

where $Y^i_{CSPI} = Y^i_{up} - Y^i_{down}$, and

$$Y^i_{CSPI} = 2I^i \int \left(A^i(x) - \frac{1}{2}\right)T(x)\mathrm{d}x + I^i_{n-up} - I^i_{n-down}, \quad \forall_i = 1, \ldots, K. \tag{5}$$

In comparison with Eq. (1), the random disturbance $Y^i_d = I^i \int T(x)\mathrm{d}x$ cased by the source's energy fluctuation is removed for the signal Y^i_{CSPI}, and thus the quality of the CSPI will be better than $O^{up}_{SPI}(x)$.

In addition, thanks to the specific structure of CSPI, the energy fluctuation of the laser can be measured by the detectors D_{up} and D_{down}, namely, $I^i \propto (Y^i_{up} + Y^i_{down}) = I^i_c$. Similar to the signal correction approach described in Ref. [21], the correction result $CSPI_{correction}$ can be expressed as

$$O_{CSPI_{correction}}(x) = \frac{1}{K}\sum_{i=1}^{K}(A^i(x) - \langle A(x)\rangle)\frac{Y^i_{CSPI}}{I^i_c}. \quad (6)$$

From Eqs. (4)–(6), it is clearly seen that the quality of CSPI will be further enhanced because the source's energy fluctuation is corrected.

In order to verify the superiority of the CSPI structure, Fig. 1(b) presents a common scheme of SPI to acquire the source's energy fluctuation for comparison, which corresponds to the SPI with signal monitoring described in Ref. [14]. We emphasize that the energy of the reflection light is divided into 50:50 by the beam splitter (BS) in Fig. 1(b). Therefore, compared with the schematic of Fig. 1(a), the light intensity detected by the detector D_t in Fig. 1(b) is half of that detected by the detector D_{up} when the other parameters are the same. What is more, the light intensity recorded by the monitor D_m is also smaller than $Y^i_{up} + Y^i_{down}$. Similar to the idea described by Eq. (6), the correction result $SPI_{correction}$ can be represented as

$$O_{SPI_{correction}}(x) = \frac{1}{K}\sum_{i=1}^{K}(A^i(x) - \langle A(x)\rangle)\frac{Y^i}{I^i_m}, \quad (7)$$

where $Y^i = \frac{1}{2}I^i\int A^i(x)T(x)\mathrm{d}x + I^i_{n-up}$, $\forall_i = 1,\ldots,K$, and $I^i_m = \frac{1}{2}I^i\int T(x)\mathrm{d}x + I^i_{n-up}$, $\forall_i = 1,\ldots,K$ is the energy fluctuation of the pulsed laser measured by the monitor in Fig. 1(b). However, in comparison with the $CSPI_{correction}$, the detection signal-to-noise ratio (DSNR) of both the signal Y^i and the monitor signal I^i_m for the method $SPI_{correction}$ is reduced because of the injection of the BS, which means that the reconstruction quality of the $SPI_{correction}$ will be worse than that of the $CSPI_{correction}$.

In order to evaluate quantitatively the quality of images reconstructed by the methods described above, the reconstruction fidelity is estimated by calculating the peak signal-to-noise ratio (PSNR),

$$\mathrm{PSNR} = 10\times\log_{10}\left(\frac{(2^p-1)^2}{\mathrm{MSE}}\right), \quad (8)$$

where the larger the value PSNR, the better the quality of the recovered image. For a 0–255 gray-scale image, $p = 8$ and MSE represents the mean square error of the reconstruction images O_{rec} with respect to the original object O, namely,

$$\mathrm{MSE} = \frac{1}{N_{pix}}\sum_{i=1}^{N_{pix}}(O_{rec}(x_i) - O(x_i))^2, \quad (9)$$

where N_{pix} is the total pixel number of the image.

3. Simulated and Experimental Results

To verify the idea, the parameters of the experimental demonstration based on the schematic of Fig. 1 are set as follows: the wavelength of the laser is 532 nm, the transverse size of the patterns at the DMD plane is set as 54.6 μm, and the modulated area of the DMD is 64 × 64 pixels (one pixel is equal to the pattern's transverse size). The speckle patterns modulated by the DMD are Hadamard patterns (where the position of the value "−1" is set as 0) and the measurement number is $K = 4096$. In addition, $z_{11} = z_{21} = 250$ mm, $z_{12} = z_{22} = 1000$ mm, and $f_1 = f_2 = 200$ mm. The imaging target, as illustrated in Fig. 3, is a "star" diagram (64 × 64 pixels, one pixel corresponds to 218.4 μm × 218.4 μm). The ideal detection signal of imaging the object "star," namely, $Y^i_t = \int A^i(x)T(x)\mathrm{d}x$, is shown in Fig. 2(a). The DSNR is usually denoted as the ratio between the ideal detection signal's ensemble average and the noise's standard deviation [namely, $\varepsilon = 10\log_{10}(\frac{\langle Y^i_t\rangle}{\mathrm{std}(I^i_{n-up})})$]. In the case of $\varepsilon = 26.5$ dB and $\delta = 0.24$, Figs. 2(b)–2(d) have given the detection signals of SPI_{up}, CSPI, $CSPI_{correction}$, and $SPI_{correction}$ based on the schematic of Figs. 1(a) and 1(b), respectively. By computing the correlation coefficient β between the signal Y_t and the signals

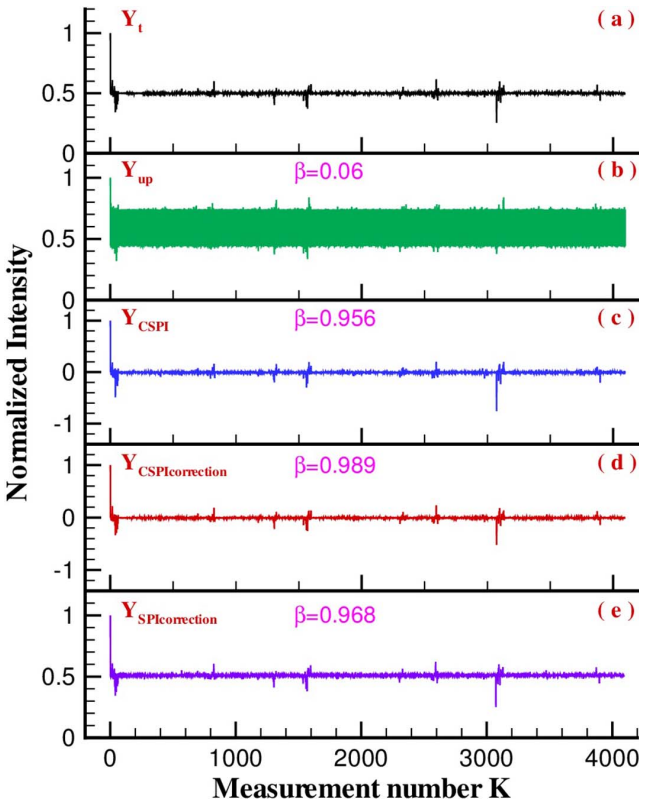

Fig. 2. Different experimental detection signals in the condition of $\varepsilon = 26.5$ dB and $\delta = 0.24$. (a) The target's ideal detection signal without noise Y_t, (b) the signal Y_{up} detected by the detector D_{up}, (c) the signal Y_{CSPI} obtained by CSPI method, (d) the signal $Y_{CSPI_{correction}} = \frac{Y^i_{CSPI}}{I^i_c}$ achieved by $CSPI_{correction}$ method, and (e) the signal $Y_{SPI_{correction}} = \frac{Y^i}{I^i_m}$ achieved by $SPI_{correction}$ method.

$Y_{up}/Y_{CSPI}/Y_{CSPI_{correction}}/Y_{SPI_{correction}}$ [26], the value β of SPI_{up} is only 0.06, whereas it approaches 1 for the $CSPI_{correction}$, which means that the reconstruction image $O^{up}_{SPI}(x)$ will be very bad, but the target's image can be perfectly recovered by $CSPI_{correction}$ method.

When the DSNR $\varepsilon = 26.5$ dB is fixed, Fig. 3 has displayed the experimental reconstruction results of $SPI_{up}/CSPI/CSPI_{correction}/SPI_{correction}$ in the condition of $\delta = 0.03$, 0.07, 0.11, 0.16, and 0.24, respectively. As shown in Figs. 3(a)–3(e), the quality of SPI_{up} is sharply decreased with the increase of the source's energy fluctuation δ (especially when $\delta < 0.07$). When the method of complementary detection is adopted, the reconstruction quality is dramatically improved by CSPI. In addition, it is clearly seen that the method of $CSPI_{correction}$, as predicted by Eq. (6), can further enhance the quality of the CSPI, especially when the value δ is greater than 0.1, because the source's energy fluctuation is corrected. What is more, similar to the results described in Ref. [14], the quality of SPI can be also enhanced when a monitor is introduced to measure the source's energy fluctuation and corresponding correction approaches is exploited. However, the reconstruction results obtained by $CSPI_{correction}$ are always much better than that of $SPI_{correction}$.

In order to further demonstrate that the CSPI structure is superior to the scheme shown in Fig. 1(b), Fig. 4 shows the performance comparison of $CSPI_{correcion}$ and $SPI_{correcion}$ at different ε and $\delta = 0.2$ by experiments based on the same parameters described in Fig. 2. Here, only the photon shot noise is considered, and the DSNR can be expressed as $\varepsilon = 10\log_{10}\sqrt{\langle Y^i_{up}\rangle}$. Therefore, the DSNR of both the signal Y^i and the monitor signal I^i_m for the method $SPI_{correction}$ is 1.5 dB lower than that of $CSPI_{correction}$ because of the injection of the BS in Fig. 1(b). It is clearly seen that $CSPI_{correcion}$ is always better than $SPI_{correcion}$, which originates from higher DSNR ε and higher precision to measure the signal's intensity fluctuation I^i for the CSPI scheme. As described above in Eq. (7), if the source's intensity for the scheme of Fig. 1(b) is twice that of Fig. 1(a), then the signal Y^i of $SPI_{correcion}$ is the same as the signal Y^i_{up} (namely, corresponding to the same DSNR ε for the two SPI schemes), and the corresponding reconstruction result of $SPI_{correcion}$ is shown in Fig. 5(b). It is observed that the quality of $SPI_{correcion}$ is improved [see Figs. 5(a) and 5(b)], but it is still worse than $CSPI_{correcion}$ with $\varepsilon = 20$ dB, which means that the signal I^i_c is much closer to the signal I^i compared with the monitor signal I^i_m. In addition, as displayed in Figs. 5(c)–5(e), the quality of SPI_{up} can be dramatically enhanced and even is the same as $CSPI_{correcion}$ when the signal I^i_c is used to correct the signal Y^i_{up}, which can be explained by Eqs. (1), (5), and (6), and further verifies the analysis above.

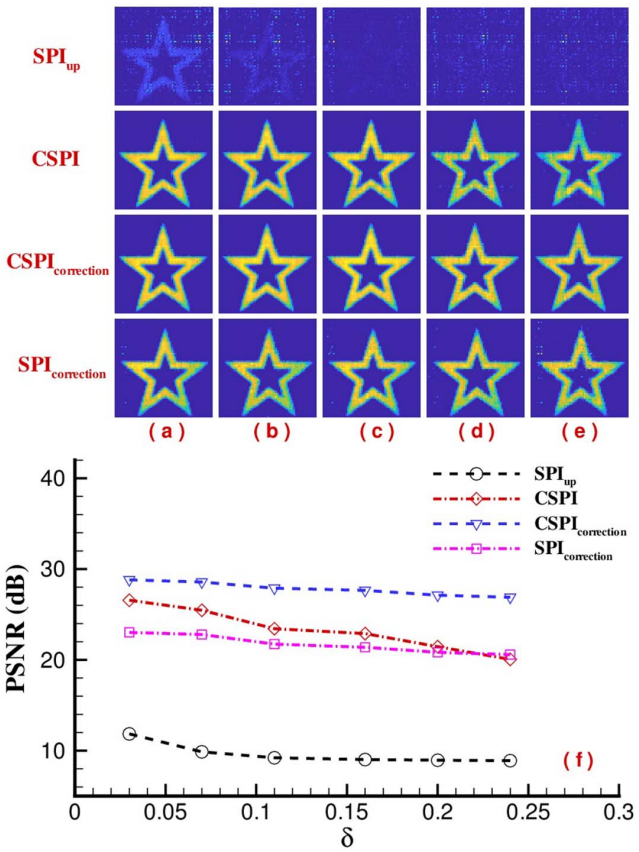

Fig. 3. Experimental demonstration of the influence of the source's energy fluctuation δ on different reconstruction SPI methods when the DSNR ε is 26.5 dB. (a) $\delta = 0.03$, (b) $\delta = 0.07$, (c) $\delta = 0.11$, (d) $\delta = 0.16$, and (e) $\delta = 0.24$. (f) The curve of PSNR-δ, where SPI_{up} is the reconstruction result based on $A^i(x)$ and Y^i_{up}, which corresponds to the conventional SPI.

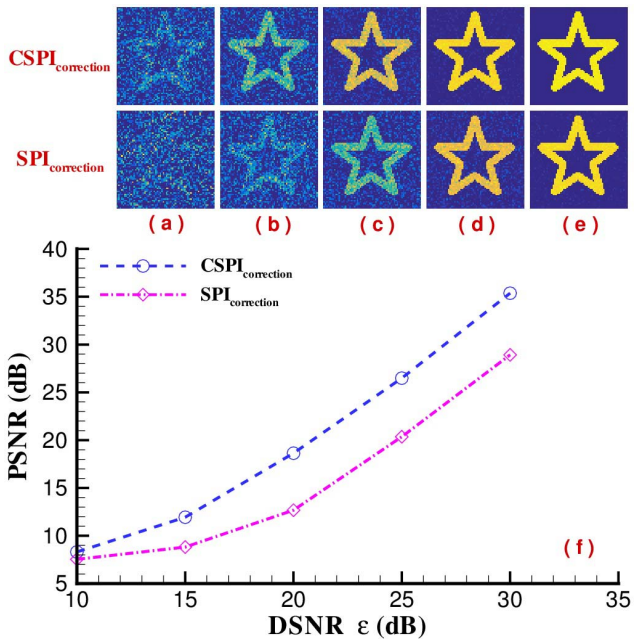

Fig. 4. Effect of DSNR ε on the results of $CSPI_{correcion}$ and $SPI_{correcion}$ when $\delta = 0.2$ is fixed. (a) $\varepsilon = 10$ dB, (b) $\varepsilon = 15$ dB, (c) $\varepsilon = 20$ dB, (d) $\varepsilon = 25$ dB, and (e) $\varepsilon = 30$ dB. (f) The curve of PSNR-ε.

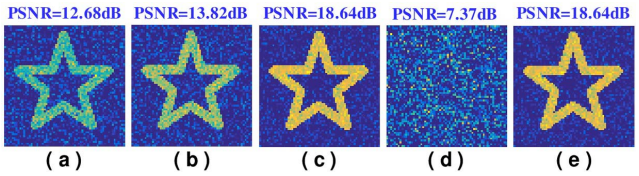

Fig. 5. Performance comparison of different correction reconstruction methods in the condition of $\delta = 0.2$. (a) $\mathrm{SPI}_{\mathrm{correction}}$ with $\varepsilon = 20$ dB, (b) $\mathrm{SPI}_{\mathrm{correction}}$ with $\varepsilon = 21.5$ dB, (c) $\mathrm{CSPI}_{\mathrm{correction}}$ with $\varepsilon = 20$ dB, (d) $\mathrm{SPI}_{\mathrm{up}}$ with $\varepsilon = 20$ dB, and (e) $\mathrm{SPI}_{\mathrm{up\text{-}correction}}$ with $\varepsilon = 20$ dB, where $\mathrm{SPI}_{\mathrm{up\text{-}correction}}$ is the reconstruction result based on $A^{l}(x)$ and $\frac{Y_{\mathrm{up}}^{l}}{I_c^{l}}$.

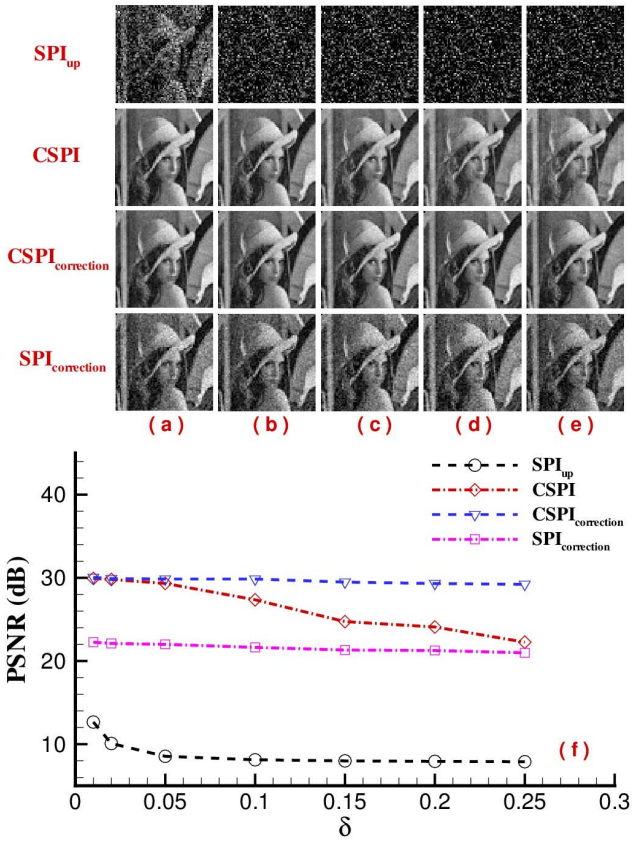

Fig. 6. Simulated demonstration of imaging a complicated image "Lena" at different δ when the DSNR ε is 28 dB. The description of (a)–(f) is the same as Fig. 3.

In order to validate the applicability of CSPI for complex scenes, Fig. 6 gives a simulation demonstration of testing a famous picture "Lena". Using the same simulation parameters as Fig. 4, except for the DSNR $\delta = 28$ dB, the results of different reconstruction methods are shown in Figs. 6(a)–6(e), and their corresponding curves of PSNR-ε are displayed in Fig. 6(f), which are similar to the experimental results described in Fig. 3. Therefore, we demonstrate that the method of $\mathrm{CSPI}_{\mathrm{correcion}}$ is robust to the source's energy fluctuation and superior to previous SPI with signal monitoring described in Fig. 1(b). In addition, similar to the results described in Ref. [14], $\mathrm{CSPI}_{\mathrm{correcion}}$ can be also used to dramatically enhance the quality of SPC in a light disturbance environment or in the case where there is intensity fluctuation between the target plane and the modulation device plane or the target itself.

4. Conclusion

In summary, we have proposed an approach that can remove the influence of the source's energy fluctuation on SPI based on complementary detection and the correction of a testing signal. We also show that the scheme of CSPI is superior to SPI with signal monitoring. This work is very helpful to SPI Lidar in remote sensing, where the energy fluctuation of the pulsed laser is usually large, and in SPI in the environment where the phenomenon of atmospheric scintillation is conspicuous.

Acknowledgements

This work was supported by the Natural Science Research of Jiangsu Higher Education Institutions of China (No. 21KJA140001), the Aeronautical Science Foundation of China (No. 2020Z073012001), and the Startup Funding of Soochow University (No. NH15901123).

References

1. J. Cheng and S. Han, "Incoherent coincidence imaging and its applicability in X-ray diffraction," Phys. Rev. Lett. **92**, 093903 (2004).
2. R. S. Bennink, S. J. Bentley, R. W. Boyd, *et al.*, "Quantum and classical coincidence imaging," Phys. Rev. Lett. **92**, 033601 (2004).
3. D.-Z. Cao, J. Xiong, and K. Wang, "Geometrical optics in correlated imaging systems," Phys. Rev. A **71**, 013801 (2005).
4. J. H. Shapiro and R. W. Boyd, "The physics of ghost imaging," Quantum Inf. Process. **11**, 949 (2012).
5. D. Graham-Rowe, "Pixel power," Nat. Photonics **1**, 211 (2007).
6. M. F. Duarte, M. A. Davenport, D. Takhar, *et al.*, "Single-pixel imaging via compressive sampling," IEEE Signal Process. Mag. **25**, 83 (2008).
7. M. P. Edgar, G. M. Gibson, and M. J. Padgett, "Principles and prospects for single-pixel imaging," Nat. Photonics **13**, 13 (2019).
8. C. A. Osorio Quero, D. Durini, J. Rangel-Magdaleno, *et al.*, "Single-pixel imaging: an overview of different methods to be used for 3D space reconstruction in harsh environments," Rev. Sci. Instrum. **92**, 111501 (2021).
9. J. H. Shapiro, "Computational ghost imaging," Phys. Rev. A **78**, 061802 (2008).
10. Y. Bromberg, O. Katz, and Y. Silberberg, "Ghost imaging with a single detector," Phys. Rev. A **79**, 053840 (2009).
11. B. Sun, M. Edgar, R. Bowman, *et al.*, "3D computational imaging with single-pixel detectors," Science **340**, 844 (2013).
12. M.-J. Sun and J.-M. Zhang, "Single-pixel imaging and its application in three-dimensional reconstruction: a brief review," Sensors **19**, 732 (2019).
13. X. Mei, W. Gong, Y. Yan, *et al.*, "Experimental research on prebuilt three-dimensional imaging Lidar," Chin. J. Lasers, **43**, 0710003 (2016).
14. W. Gong, "Performance comparison of computational ghost imaging versus single-pixel camera in light disturbance environment," Opt. Laser Technol. **152**, 108140 (2022).
15. K. Shibuya, K. Nakae, Y. Mizutani, *et al.*, "Comparison of reconstructed images between ghost imaging and Hadamard transform imaging," Opt. Rev. **22**, 897 (2015).
16. C. Wang, W. Gong, X. Shao, *et al.*, "The influence of the property of random coded patterns on fluctuation-correlation ghost imaging," J. Opt. **18**, 065703 (2016).
17. Z. Zhang, X. Ma, and J. Zhong, "Single-pixel imaging by means of Fourier spectrum acquisition," Nat. Commun. **6**, 6225 (2015).

18. Z. Zhang, X. Wang, G. Zheng, *et al.*, "Hadamard single-pixel imaging versus Fourier single-pixel imaging," Opt. Express **25**, 19619 (2017).
19. M.-J. Sun, L.-T. Meng, M. P. Edgar, *et al.*, "A Russian Dolls ordering of the Hadamard basis for compressive single-pixel imaging," Sci. Rep. **7**, 3464 (2017).
20. C. Zhou, T. Tian, C. Gao, *et al.*, "Multi-resolution progressive computational ghost imaging," J. Opt. **21**, 055702 (2019).
21. X. Mei, C. Wang, Y. Fang, *et al.*, "Influence of the source's energy fluctuation on computational ghost imaging and effective correction approaches," Chin. Opt. Lett. **18**, 042602 (2020).
22. W.-K. Yu, X.-F. Liu, X.-R. Yao, *et al.*, "Complementary compressive imaging for the telescopic system," Sci. Rep. **4**, 5834 (2014).
23. B.-B. Luo, K.-C. Tsai, and J.-P. Liu, "Computational ghost imaging by using complementary illumination patterns," Proc. SPIE **10711**, 107111W (2018).
24. W. Gong, "Disturbance-free single-pixel imaging camera via complementary detection," Opt. Express **31**, 30505 (2023).
25. J. W. Goodman, *Introduction to Fourier Optics* (McGraw-Hill, 1968).
26. Z. Li, Q. Zhao, and W. Gong, "Distorted point spread function and image reconstruction for ghost imaging," Opt. Laser Eng. **139**, 106486 (2021).